ADVANCING EARTH AND SPACE SCIENCES

JGR Space Physics

RESEARCH ARTICLE
10.1029/2026JA035335

Key Points:
- MMS observations show asymmetric Hall magnetic field structures in guide-field magnetopause reconnection
- The southward jet exhibits a tripolar structure, whereas the northward jet exhibits a bipolar structure
- The results are consistent with the previous particle-in-cell simulations of asymmetric guide-field reconnection

Correspondence to:
W.-L. Teh,
waileong.teh@gmail.com

Citation:
Teh, W.-L., Shu, Y., & Lu, Q. (2026). Asymmetric Hall magnetic field structures in oppositely directed jets during guide-field magnetopause reconnection. *Journal of Geophysical Research: Space Physics*, *131*, e2026JA035335. https://doi.org/10.1029/2026JA035335

Received 10 MAR 2026
Accepted 18 AUG 2026

Author Contributions:
Conceptualization: Wai-Leong Teh, Yukang Shu, Quanming Lu
Formal analysis: Wai-Leong Teh
Investigation: Wai-Leong Teh, Yukang Shu, Quanming Lu
Methodology: Wai-Leong Teh
Supervision: Wai-Leong Teh
Validation: Wai-Leong Teh, Yukang Shu, Quanming Lu
Visualization: Wai-Leong Teh
Writing – original draft: Wai-Leong Teh
Writing – review & editing: Wai-Leong Teh

Asymmetric Hall Magnetic Field Structures in Oppositely Directed Jets During Guide-Field Magnetopause Reconnection

Wai-Leong Teh[1], Yukang Shu[2], and Quanming Lu[2]

[1]Space Science Center, Institute of Climate Change, Universiti Kebangsaan Malaysia, Bangi, Malaysia, [2]School of Earth and Space Sciences/Deep Space Exploration Laboratory, University of Science and Technology of China, Hefei, China

Abstract Symmetric Hall magnetic field structures, such as bipolar or quadrupolar patterns, are commonly expected around a single magnetic X-line during asymmetric guide-field reconnection. In such cases, oppositely directed reconnection jets are generally associated with the same number of Hall magnetic field polarities. Here, we report for the first time Magnetospheric Multiscale (MMS) observations of asymmetric Hall magnetic field structures in oppositely directed magnetopause reconnection jets. We validate a method for estimating Hall magnetic fields from in-plane electric currents using virtual spacecraft measurements from particle-in-cell (PIC) simulations of symmetric reconnection. We then examine three magnetopause reconnection events (G1, G2, and G3) with substantial guide fields (26%, 48%, and 79% of the reconnecting field). The G1 and G2 events exhibit northward and southward jets, respectively, while G3 shows a bipolar jet. Their upstream magnetic field and density ratios (magnetosphere to magnetosheath) are G1: (1.4, 0.17), G2: (1.3, 0.19), and G3: (1.6, 0.09), where the first value in each pair represents the magnetic field ratio and the second the density ratio. Despite comparable upstream conditions for G1 and G2, their Hall magnetic field structures differ: the southward jet exhibits a tripolar structure $(+, -, +)$, whereas the northward jet shows a bipolar structure $(+, -)$, with the negative polarity located on the magnetospheric side. In G3, a tripolar structure $(+, -, +)$ is also observed in the southward jet, whereas the northward jet shows only positive Hall magnetic field polarity. These observations agree with predictions from previous PIC simulations of asymmetric guide-field reconnection.

Plain Language Summary Collisionless magnetic reconnection is a fundamental process in astrophysical plasma that converts magnetic field energy into the kinetic and thermal energies of plasma. A key signature of this process is the generation of out-of-plane Hall magnetic fields produced by Hall current loops. Traditionally, the polarities of these Hall magnetic fields are expected to be symmetric in the oppositely directed reconnection outflows. In this study, however, we demonstrate for the first time that this symmetric Hall magnetic field pattern does not persist during guide-field magnetopause reconnection events observed by MMS.

1. Introduction

Collisionless magnetic reconnection is a fundamental plasma process that transports solar wind energy into the Earth's magnetosphere. In this regime, Hall magnetic and electric fields arise within the ion diffusion region due to the decoupled motions of ions and electrons (e.g., Sonnerup, 1979). Over the past two decades, such Hall fields have been widely observed in the ion diffusion region during both magnetotail and magnetopause reconnection events. (e.g., J. P. Eastwood et al., 2010, 2013; X. Li et al., 2025; F. S. Mozer et al., 2008; F. S. Mozer et al., 2002; T. Nagai et al., 2001; M. Øieroset et al., 2001; S. Y. Tang et al., 2021; W.-L. Teh et al., 2010, 2011, 2014; R. S. Wang et al., 2012, 2017; Y. C. Zhang et al., 2017; M. Zhou et al., 2018).

For symmetric reconnection without a guide field, where the upstream magnetic field strength and plasma density are identical on both sides, the Hall magnetic field exhibits a well-known quadrupolar pattern generated by Hall current loops, while the Hall electric field displays a bipolar pattern (e.g., J. Birn et al., 2001; P. L. Pritchett, 2001; M. A. Shay et al., 2001; X. R. Fu et al., 2006; Q. M. Lu et al., 2010; S. Lu et al., 2011). When a substantial guide field is present, this quadrupolar pattern becomes distorted (e.g., S. Lu et al., 2011).

For asymmetric reconnection without a guide field, the Hall magnetic field may exhibit either a bipolar or quadrupolar pattern (e.g., M. A. Shay et al., 2016; L. Dai, 2018; L. L. Sang et al., 2018, 2019a). Additionally, a hexapolar pattern was identified by L. L. Sang et al. (2018, 2019a) in two-dimensional (2D) PIC simulations of asymmetric reconnection without a guide field. This hexapolar pattern evolves from the quadrupolar pattern. In the previous simulations, bipolar, quadrupolar, and hexapolar patterns are considered symmetric Hall magnetic field structures because they exhibit the same number of Hall magnetic field polarities (or signs) on the left and right sides of an X-line; for example, a quadrupolar pattern has two polarities on each side of the X-line.

Later, L. L. Sang et al. (2019b) reported asymmetric Hall magnetic field structures in 2D PIC simulations of asymmetric reconnection with substantial guide fields (B_g). The Hall magnetic fields (i.e., $B_M - B_g$) exhibit a tripolar structure (+, −, +) on the left side of the X-line and a bipolar structure (+, −) on the right side, with the negative polarity located on the magnetospheric side. Here B_M denotes the out-of-plane magnetic field component. This configuration is neither quadrupolar nor hexapolar. However, such asymmetric Hall magnetic field structures have not yet been confirmed by spacecraft observations.

In this study, we present the first observational evidence of asymmetric Hall magnetic field structures during guide-field magnetopause reconnection using spacecraft data from MMS (J. L. Burch et al., 2016). We analyze three magnetopause reconnection events (G1, G2, and G3) with substantial guide fields. The G1 and G2 events exhibit northward and southward jets, respectively, whereas G3 shows a bipolar jet. We validate a method for estimating Hall magnetic fields from in-plane electric currents using virtual spacecraft data from symmetric reconnection simulation and then apply this method to the three events to identify the associated Hall magnetic field structures.

2. Hall Magnetic Field Estimate and Results

For a 2D magnetic field structure, the magnetic field vector can be expressed as $\mathbf{B} = \nabla A \times \hat{m} + \hat{m}B_M$, where A is the magnetic vector potential, $\hat{m}$ is the invariant axis (i.e., $\partial/\partial m = 0$), and $\nabla = \hat{l}\partial/\partial l + \hat{n}\partial/\partial n$. In a 2D reconnection configuration, the unit vectors $\hat{l}$ and $\hat{n}$ are directed along the reconnecting magnetic field and the normal direction, respectively. From Ampère's law, the electric current density is given by

$$\mathbf{j} = 1/\mu_0\left(\nabla B_M \times \hat{m} - \hat{m}\nabla^2 A\right). \tag{1}$$

To first order, the differential of the out-of-plane magnetic field component is given as $dB_M \approx (\partial B_M/\partial l)\,dl + (\partial B_M/\partial n)\,dn$. Using the relationships $\partial B_M/\partial n = -\mu_0 j_L$ and $\partial B_M/\partial l = \mu_0 j_N$, the B_M perturbation is then estimated along the spacecraft trajectory as follows:

$$\Delta B_M = -\mu_0\int_{t_1}^{t_2} j_L u_n dt + \mu_0\int_{t_1}^{t_2} j_N u_l dt = B_{\mathrm{H}}, \tag{2}$$

Here, u_n and u_l are constant representing the spacecraft's velocities along the n- and l- directions, respectively, relative to the current sheet. These velocities are used to compute the dl and dn. Equation 2 estimates the out-of-plane magnetic field perturbation, that is, the Hall magnetic field, $B_{\mathrm{H}} = B_M - B_g = \Delta B_M$, using the in-plane current densities j_L and j_N. The guide field B_g is assumed to be spatially uniform. These in-plane currents form the so-called Hall current loop within the ion diffusion region. Depending on the local magnetic field configuration, the in-plane Hall current may be either perpendicular or parallel to the in-plane magnetic field. In the ion diffusion region, the current density j_L plays a dominant role in generating the Hall magnetic field B_{H}. In this study, the measured current density is calculated as $\mathbf{j} = en_e(\mathbf{V}_i - \mathbf{V}_e)$, where e is the elementary charge, n_e is the electron density, and $\mathbf{V}_i$ and $\mathbf{V}_e$ are the ion and electron plasma velocities, respectively.

A 2D PIC simulation of symmetric reconnection is used to validate the Hall magnetic field estimation method based on Equation 2. We note that the simulation is used solely for methodological validation and not for quantitative comparison with the MMS observations. The initial magnetic field configuration is an 1D Harris current sheet in the x-z plane, given by $\mathbf{B} = B_0 \tanh(z/\delta)\,\hat{x} + B_{\mathrm{g}}\,\hat{y}$, where $\delta = 0.5\ d_i$ is the half-width of the current sheet and $d_i = c/\omega_{pi}$ is the ion inertial length, which is the ratio of the speed of light to the ion plasma frequency. The initial plasma density profile is expressed as $\rho = \rho_0\,\mathrm{sech}^2(z/\delta) + \rho_b$, with $\rho_b = 0.2\,\rho_0$ representing the background density in terms of the initial density ρ_0 at the center of the current sheet. The simulation box dimension is $L_x \times L_z = 204.8\ d_i \times 25.6\ d_i$, with grid spacing $\Delta x = \Delta z = 0.05\ d_i$. The simulation time step is

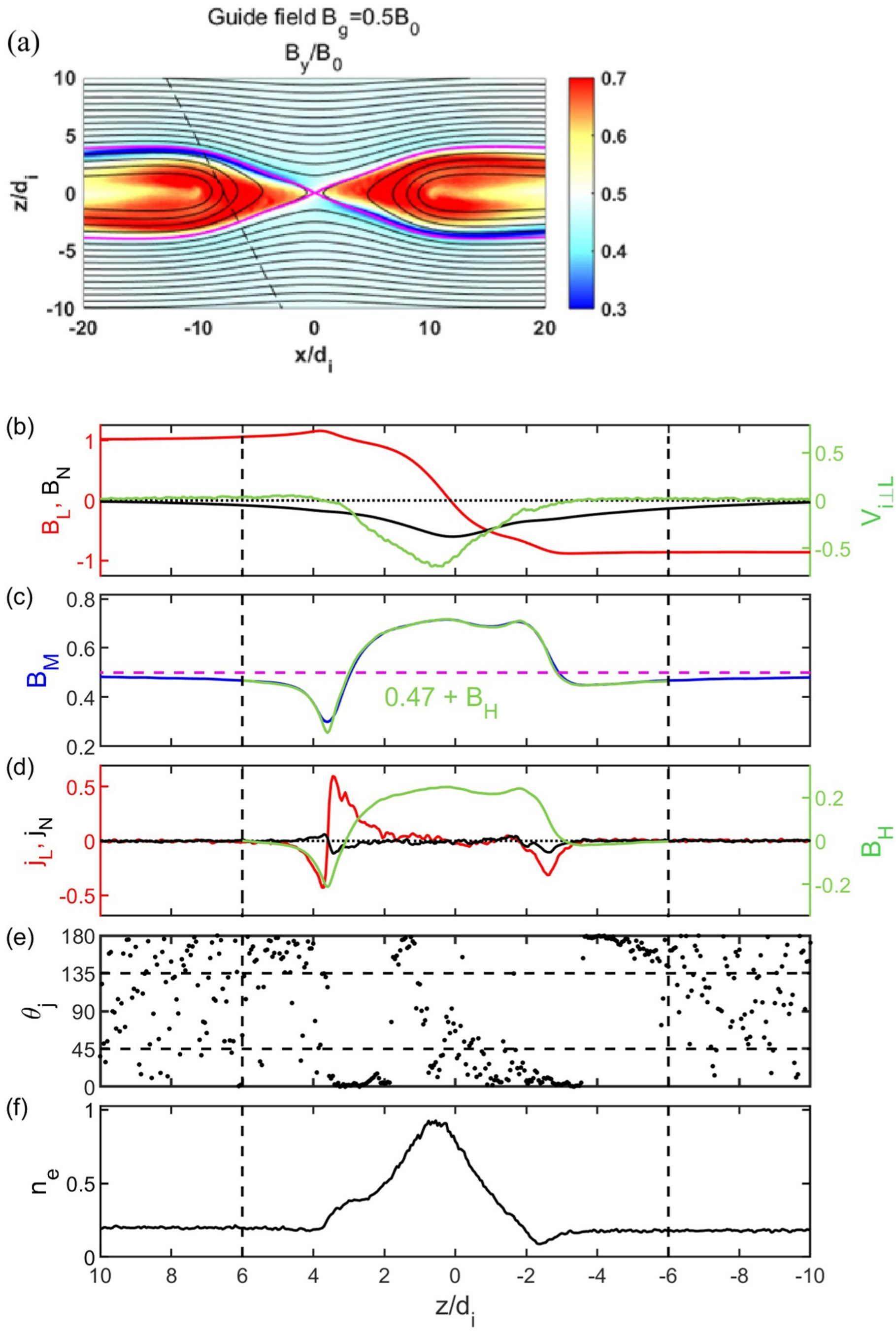

Figure 1. (a) Magnetic field map for symmetric guide-field reconnection, with the out-of-plane magnetic field B_y shown in color. The magenta lines indicate the reconnection separatrices. (b–f) Simulated data along a spacecraft trajectory (the dashed line) shown in (a), along with the estimated Hall magnetic field B_H and the angle θ_j between the in-plane current density vector and the in-plane magnetic field. The magenta line in panel (c) denotes the initial guide field of 0.5.

$0.001\ \Omega_i^{-1}$, where Ω_i is the ion cyclotron frequency. The mass ratio m_i/m_e is set to 100. The simulation data used in this study were provided by Y. K. Shu et al. (2022).

Figure 1a shows the magnetic field configuration in the x-z plane for $B_g/B_0 = 0.5$ at $\Omega_i t = 49$, with the out-of-plane B_y field represented in color. The (x, y, z) axes correspond to the (l, m, n) axes, respectively. In the figure, the reconnection separatrices are indicated by the magenta lines and the black dashed line represents the virtual spacecraft trajectory passing through the ion diffusion region and the current sheet. The simulated data along the spacecraft trajectory is presented in Figures 1b–1f. Figure 1b displays the B_L, B_N, and $V_{i\perp L}$, revealing the reconnection jet within the current sheet, accompanied by a significant normal magnetic field component. The $V_{i\perp L}$ denotes the L-component of the ion velocity perpendicular to the magnetic field. The B_{H} field between the two dashed lines is estimated by Equation 2, using $dl = 0.025$ and $dn = -0.05$. A bipolar structure is observed (see Figure 1d), characterized by negative B_{H} around $z/d_i = 4$ and positive B_{H} within the current layer. The negative peak in B_{H} coincides with the reversal point of the bipolar j_L current. Figure 1e shows the angle θ_j between the in-plane current density vector and the in-plane magnetic field. It can be seen that the regions of large current density are predominantly field-aligned. Good agreement is obtained between B_M and $B_{\mathrm{H}}+ 0.47$ (see Figure 1c), where the offset of 0.47 corresponds to the B_M value at the location of the first dashed line and represents the guide field. This comparison demonstrates that Equation 2 provides an accurate estimate of the Hall magnetic field resulting from 2D reconnection, as expected. Similar agreement is also found for symmetric reconnection cases with $B_g/B_0 = 0$ and 1.0 (not shown). We note that although Equation 2 is validated using a symmetric reconnection simulation, its applicability extends to asymmetric reconnection because it is derived from the Ampère's law.

3. MMS Event Studies

Three guide-field magnetopause reconnection events (G1, G2, and G3) observed by the MMS spacecraft are presented. Northward and southward reconnection jets are observed for G1 and G2, respectively, while G3 shows a bipolar jet. Measurements of magnetic fields from the Fluxgate Magnetometer (C. T. Russell et al., 2016), electric fields from Electric Double Probe (P.-A Lindqvist et al., 2016), and electron density, as well as ion and electron plasma velocities from the Fast Plasma Instrument (C. Pollock et al., 2016), are used at burst mode resolution. Vector components are shown in geocentric solar ecliptic (GSE) coordinates.

Figure 2 presents the analysis results of the northward jet (the G1 event) observed by MMS1 during the interval from 10:31:12 to 10:31:30 UT on 13 December 2015. This event was previously studied by Y. C. Zhang et al. (2017) estimated Hall magnetic fields using the Biot-Savart law, a method different from ours. The two vertical lines in the figure indicate the locations of the upstream magnetic fields: $\mathbf{B}_1 = (-15.4, 15.1, -20.2)$ nT, located in the magnetosheath, and $\mathbf{B}_2 = (9.2, -8.1, 39.1)$ nT, located in the magnetosphere. The magnetic shear angle across the magnetopause is approximately 150°. These $\mathbf{B}_1$ and $\mathbf{B}_2$ magnetic fields are then used to estimate the m axis, calculated as:

$$\hat{m} = (\mathbf{B}_1 \times \mathbf{B}_2) \times (\mathbf{B}_1 - \mathbf{B}_2)/|(\mathbf{B}_1 \times \mathbf{B}_2) \times (\mathbf{B}_1 - \mathbf{B}_2)| = (0.598,\ -0.630,\ -0.495).$$

The normal axis is defined as $\hat{n} = \mathbf{B}_1 \times \mathbf{B}_2 / |\mathbf{B}_1 \times \mathbf{B}_2| = (0.716, 0.697, -0.023)$ (i.e., the cross-product normal), and $\hat{l} = \hat{m} \times \hat{n} = (0.360, -0.341, 0.868)$. Compared with the LMN coordinate system of Y. C. Zhang et al. (2017), the corresponding L, M, and N axes differ by approximately 6°, 17°, and 16°, respectively. The reconnection guide field is therefore calculated as $\mathbf{B}_1 \cdot \hat{m} = \mathbf{B}_2 \cdot \hat{m} = -8.7$ nT (duskward) (see the magenta line in Figure 2b), which corresponds to ~26% of the effective reconnecting magnetic field $B_{Le} = 2|B_{L1}|B_{L2}/(|B_{L1}|+B_{L2}) = 33.1$ nT, where $B_{L1} = -28.3$ nT and $B_{L2} = 40.0$ nT. The upstream conditions of the magnetopause are as follows: the ratio of the magnetic fields is $B_{L2}/|B_{L1}| = 1.4$, and the ratio of the electron densities is $n_{e2}/n_{e1} = 1.6/9.4 = 0.17$.

Figure 3a displays the measured electric fields (black), $-\mathbf{V}_i \times \mathbf{B}$ (blue), and $-\mathbf{V}_e \times \mathbf{B}$ (red) in LMN coordinates for G1. The discrepancy between $-\mathbf{V}_i \times \mathbf{B}$ and $-\mathbf{V}_e \times \mathbf{B}$ within the regions of interest, enclosed by the two black dashed lines, indicates the presence of the ion diffusion region. Despite large fluctuations in the measured electric fields, $-\mathbf{V}_e \times \mathbf{B}$ remains in qualitative agreement with the measurements.

Near the center ($B_L = 0$) of the current sheet, a northward jet ($V_{i\perp L} > 0$) with a peak speed of ~134 km/s is seen, accompanied by a negative normal magnetic field component that peaks at ~−7.7 nT (see Figure 2a). The negative normal magnetic field aligns with expectations for the northern quadrants of a magnetic X-line at the magnetopause. As shown in Figure 2c, the Hall magnetic field B_{H} is estimated by Equation 2, using $u_n = -40$ km/s and $u_l = -9$ km/s. These velocities are determined by optimizing the agreement between the observed and estimated results (see Figure 2b). The negative u_n aligns with the spacecraft motion from the magnetosheath to magnetosphere. For comparison, the timing analysis based on the B_L reversal yields an estimated $|u_n|$ of ~65 km/s (Y. C. Zhang et al., 2017), exceeding our result. The width of the ion diffusion region in the normal direction is estimated as 40 km/s × 12.5 s = 500 km (~6.8 d_i), where $d_i = 74$ km is the ion inertial length based on the

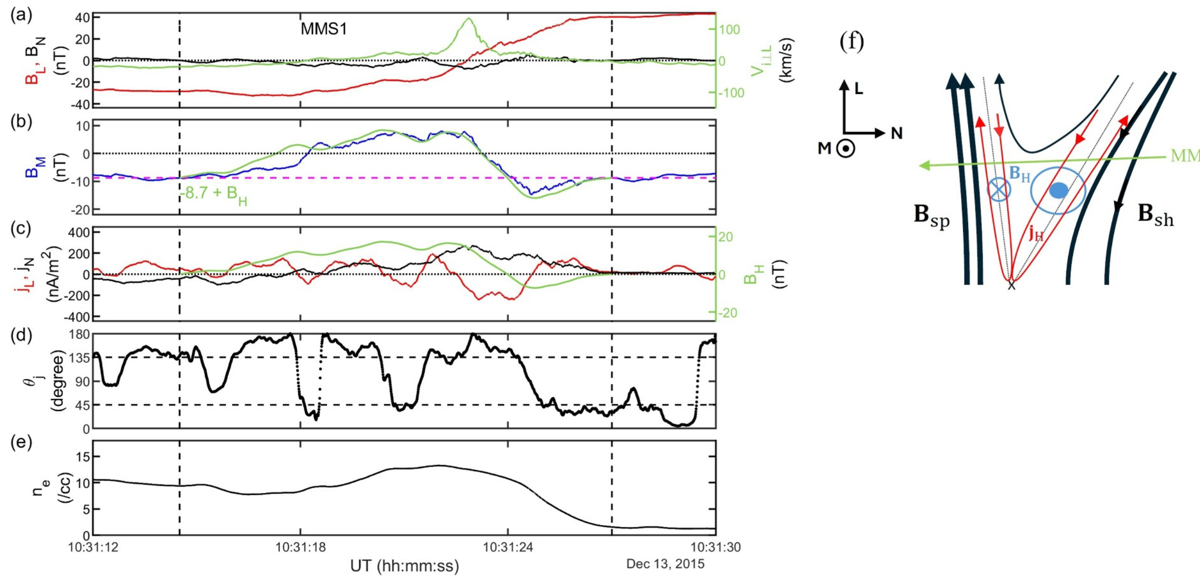

Figure 2. Analysis results for the northward reconnection jet event (G1) observed by MMS1 at the magnetopause, with the same format as Figures 1b–1f. The two vertical dashed lines mark the times 10:31:14.5 UT and 10:31:27 UT for the B_H estimate. The magenta line in panel (b) denotes the guide field of −8.7 nT. Panel (f) shows a schematic of the observed Hall magnetic field structures generated by Hall current (j_H) loops (the red lines) in the northward jet during guide-field magnetopause reconnection, with the MMS spacecraft traversing from the magnetosheath to the magnetosphere.

magnetosheath density of 9.4 cm^{-3}. A bipolar structure (+, −) is evident in Figure 2c, with the negative polarity located on the magnetospheric side. The peaks in B_H coincide with the reversal points of the bipolar j_L currents. As indicated by θ_j in Figure 2d, the in-plane Hall currents contain both perpendicular and field-aligned components relative to the in-plane magnetic fields. Figure 2f shows a schematic of the observed Hall magnetic field structures generated by Hall current (j_H) loops (the red lines) in the northward jet during guide-field magnetopause reconnection, consistent with the PIC simulation results of L. L. Sang et al. (2019b).

The G2 event, featuring a southward jet, is shown in Figure 4. It occurred on 21 October 2015, during the interval 15:10:51–15:10:57 UT. This event was previously studied by S. Y. Tang et al. (2021) identified the hexapolar Hall magnetic field pattern. The LMN coordinates are: $\hat{l} = (0.197, 0.234, 0.952)$, $\hat{m} = (0.273, -0.946, 0.176)$, and $\hat{n} = (0.942, 0.226, -0.250)$, derived using $\mathbf{B}_1 = (-11.5, 9.9, -38.3)$ nT in the magnetosheath and $\mathbf{B}_2 = (4.7, 29.1, 39.8)$ nT in the magnetosphere, which form a shear angle of 129°. Note that the m- and n- axes have been rotated by 3° about the l axis to obtain a positive average B_N. Compared with the LMN coordinate system of S. Y. Tang et al. (2021) showed that the corresponding L, M, and N axes differ by approximately 3°,11° and 11°, respectively. The reconnection guide field is −19.3 nT (duskward), corresponding to ~0.48 B_{Le}, where $B_{Le} = 40.5$ nT. The ratio $B_{L2}/|B_{L1}|$ is 45.6/36.4 = 1.3 and the ratio $n_{e2}/n_{e1} = 2.3/11.9 = 0.19$. These asymmetric ratios resemble those in the G1 event, although the guide field in the G2 event is substantially larger. As shown in Figure 3b, the ion diffusion region is characterized by the deviation between $-\mathbf{V}_i \times \mathbf{B}$ and $-\mathbf{V}_e \times \mathbf{B}$.

A southward reconnection jet, peaking at ~ −279 km/s, is observed in the current sheet (see Figure 4a), along with a small average B_N (~0.42 nT). This positive B_N is expected for the southern quadrants of a magnetic X-line at the magnetopause. Unlike the G1 event, a significant shear flow in the L-direction is observed at the magnetopause. The B_H fields, estimated from the in-plane currents, are in reasonable agreement with the observations (see Figure 4b). For the calculation, u_n = 130 km/s and u_l = 40 km/s are used. For comparison, the estimated u_n from the timing analysis is ~51 km/s (S. Y. Tang et al., 2021), which is significantly smaller than our result. The positive u_n aligns with the spacecraft motion from the magnetosphere to magnetosheath. The width of the ion diffusion region is estimated as 130 km/s × 3.2 s = 416 km (~6.3 d_i), where d_i = 66 km is based on the magnetosheath density of 11.9 cm^{-3}. Notably, the Hall magnetic fields associated with the southward jet exhibit a tripolar structure (+, −, +) (see Figure 4c), in contrast to the bipolar structure seen in the northward jet. The three $|B_H|$ peaks are located at the reversal points of the bipolar j_L currents, where both perpendicular and field-aligned Hall current components are observed (see Figure 4d). Figure 4f shows a schematic of the observed Hall magnetic

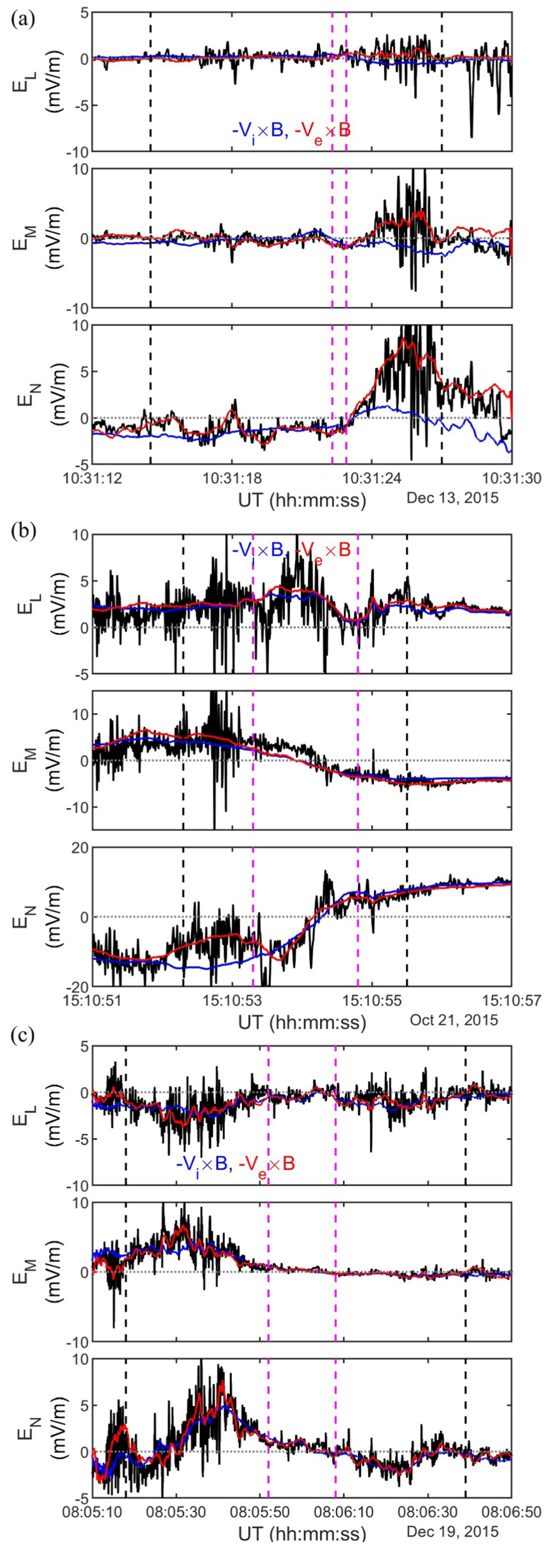

Figure 3. Comparison of the measured electric field (black), $-\mathbf{V}_i \times \mathbf{B}$ (blue), and $-\mathbf{V}_e \times \mathbf{B}$ (red) for (a) G1, (b) G2, and (c) G3 events. The vertical magenta lines indicate the analysis interval used in the method of Sonnerup and Hasegawa (2005).

field structures generated by Hall current loops in the southward jet during guide-field magnetopause reconnection, consistent with the predictions of L. L. Sang et al. (2019b). Compared with Figure 2f, an additional Hall current loop appears on the magnetosheath side of the current sheet.

The G3 event, which features a bipolar reconnection jet, is shown in Figure 5. It occurred on 19 December 2015 during the interval 08:05:10–08:06:50 UT. The LMN coordinates are: $\hat{l} = (0.223, 0.266, 0.938)$, $\hat{m} = (0.268, -0.942, 0.204)$, and $\hat{n} = (0.937, 0.206, -0.281)$, derived using $\mathbf{B}_1 = (0.9, -25.2, -15.6)$ nT in the magnetosheath and $\mathbf{B}_2 = (13.2, -10.4, 36.6)$ nT in the magnetosphere, which form a shear angle of 104°. The ratio $B_{L2}/|B_{L1}|$ is $34.5/21.1 = 1.6$ and the ratio n_{e2}/n_{e1} is $1.8/19.6 = 0.09$. During the magnetopause crossing from the magnetosphere to the magnetosheath, a southward jet is first observed on the magnetospheric side, followed by a northward jet on the magnetosheath side (see Figure 5a). One can see that a negative B_N is observed in the southward jet, which is unexpected. Attempts to obtain a positive B_N by rotating the LMN coordinate system about the L and M axes were unsuccessful. The origin of this negative B_N remains unknown, similar to the observation reported by Burch and Phan (2016). The reconnection guide field is ~20.8 nT (dawnward), corresponding to ~0.79 B_{Le}, where $B_{Le} = 26.2$ nT. The ion diffusion region is observed during the magnetopause crossing (see Figure 3c). The time interval used for the B_{H} estimation is divided into three segments, indicated by the red, black, and cyan bars in Figure 5b. The three intervals were selected based on the observed reconnection outflow signatures. Specifically, the first and third intervals correspond to the southward and northward reconnection jets, respectively, while the second interval corresponds to the jet-reversal region between the two jets. These intervals were selected within the corresponding physical regions where the estimated Hall magnetic fields showed good agreement with the observations. The resulting (u_n, u_l) values are (25 km/s, 25 km/s), (10 km/s, 15 km/s), and (15 km/s, −27 km/s) for the red, black, and cyan bars, respectively. The widths of the ion diffusion region for the three intervals are 25 km/s × 22 s = 550 km (~10.8 d_i), 10 km/s × 11.5 s = 115 km (~2.3 d_i), and 15 km/s × 37 s = 555 km (~10.9 d_i), where $d_i = 51$ km is based on the magnetosheath density of 19.6 cm^{-3}. For comparison, the u_n estimated from the timing analysis is ~31 km/s, based on the B_L reversal. This positive u_n agrees with the spacecraft motion from the magnetosphere to the magnetosheath. The spacecraft motion along the l axis is initially upward and later downward. A sketch in Figure 5f illustrates the spacecraft trajectory (green curve) within the diffusion region of the asymmetric guide-field reconnection. As shown in Figure 5c, a tripolar structure (+, −, +) also appears in the B_{H} for the southward jet (red bar), and the corresponding j_L profile resembles that of the G2 event shown in Figure 4c. For the northward jet (cyan bar), only positive B_{H} is observed. Moreover, the positive B_{H} also appears around the jet-reversal interval (black bar).

4. Summary and Discussion

We analyzed Hall magnetic field structures within northward and southward magnetopause reconnection jets from three MMS events (G1, G2, and G3). The G1 and G2 events exhibit northward and southward jets, respectively, while G3 shows a bipolar jet. Their upstream magnetic field and density ratios (magnetosphere to magnetosheath) are as follows: G1: (1.4, 0.17),

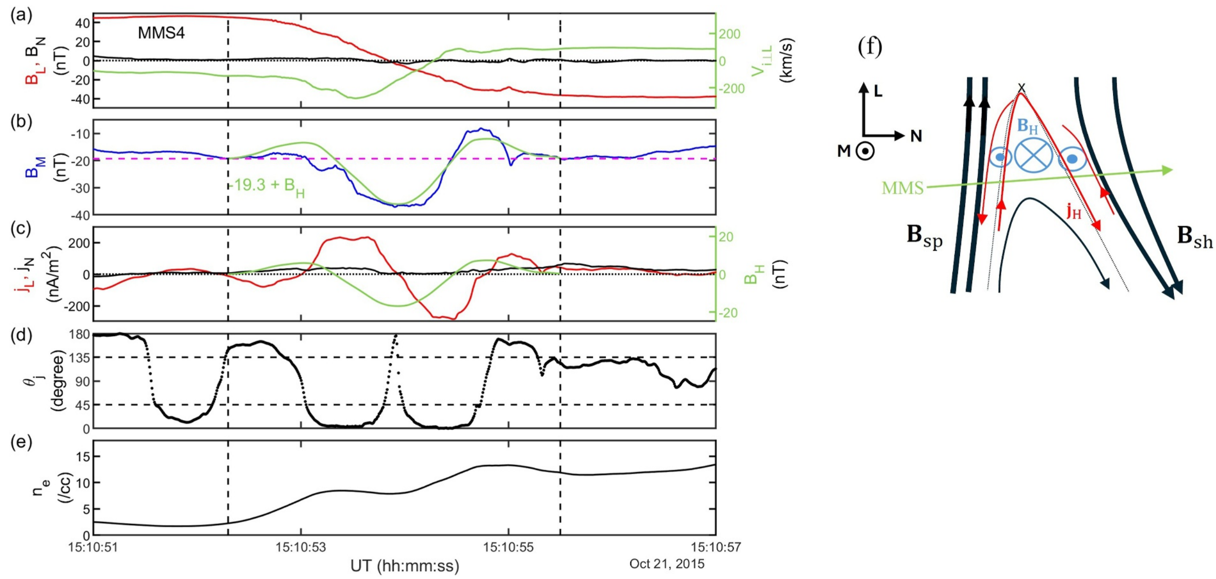

Figure 4. Analysis results for the southward reconnection jet event (G2) observed by MMS4 at the magnetopause, with the same format as Figure 2. The two vertical dashed lines mark the times 15:10:52.3 UT and 15:10:55.5 UT for the B_H estimate. The magenta line in panel (b) denotes the guide field of −19.3 nT. Panel (f) shows a schematic of the observed Hall magnetic field structures generated by Hall current loops in the southward jet during guide-field magnetopause reconnection, with the MMS spacecraft traversing from the magnetosphere to the magnetosheath.

G2: (1.3, 0.19), and G3: (1.6, 0.09). The reconnection guide fields at G1, G2, and G3 are substantial, corresponding to 26%, 48%, and 79% of the reconnecting field, respectively. The Hall magnetic field estimates show good agreement with the observations. Despite comparable upstream conditions for G1 and G2, their Hall magnetic field structures differ: the southward jet exhibits a tripolar structure (+, −, +), whereas the northward jet displays a bipolar structure (+, −), with the negative polarity located on the magnetospheric side. In G3, a tripolar structure (+, −, +) also occurs within the southward jet, while only positive Hall magnetic field polarity is observed in the

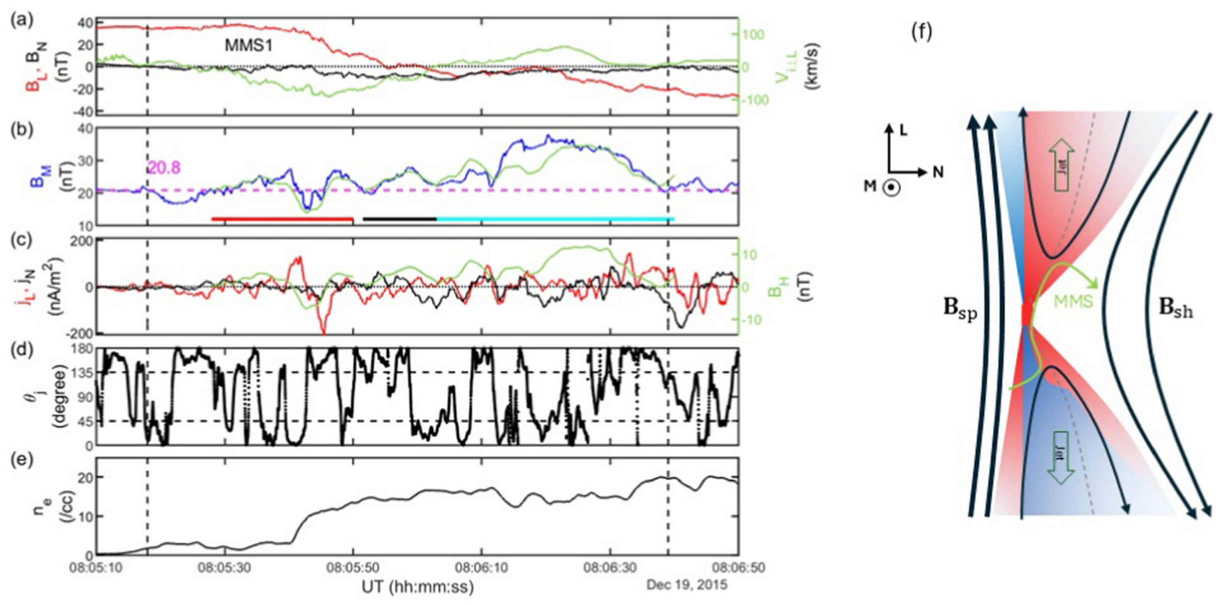

Figure 5. Analysis results for the bipolar jet event (G3) observed by MMS1 at the magnetopause, with the same format as Figure 2. In panel (b), the red, black, and cyan bars denote the three segments for the B_H estimate, and the guide field of 20.8 nT is shown by the dashed line. A sketch of the asymmetric Hall magnetic field patterns in guide-field magnetopause reconnection is shown in panel (f), along with the MMS spacecraft trajectory from the magnetosphere to the magnetosheath for this event. The red and blue color codes indicate the positive and negative Hall magnetic field polarities, respectively.

Table 1
SH05 Results for the Three Event Studies

	G1	G2	G3
$\hat{k}$ (GSE)	(0.018, −0.868, −0.496)	(0.320, −0.931, 0.178)	(-0.139, −0.972, 0.187)
$\mathbf{V}_0$ (km/s)	(74.4, −30.7, 56.3)	(−229.0, −170.2, −478.0)	(−21.7, −0.4, −18.3)
u_n, u_l (km/s)	−30.6 ± 3.4, −86.1 ± 13.3 (−40.0, −9.0)[a]	134.5 ± 13.6, 540.0 ± 15.1 (130.0, 40.0)[a]	15.3 ± 3.9, 22.1 ± 9.2 (10.0, 15.0)[b]
E_0 (mV/m)	−0.247 ± 0.025	1.904 ± 0.057	0.090 ± 0.010
ϕ_m (degree)	36.5 ± 0.6	2.8 ± 1.8	23.6 ± 0.8

[a]Results of u_n and u_l based on Equation 2. [b]Results of u_n and u_l based on Equation 2 for the black bar.

northward jet. Overall, these observational results indicate that the number of Hall magnetic field polarities is not identical for the oppositely directed jets in the asymmetric guide-field reconnection, as predicted by L. L. Sang et al. (2019b).

In the Hall magnetic field estimation for the three events, the speed u_n based on Equation 2 differs from that obtained using the timing method based on the B_L reversal. To further examine the speeds u_n and u_l, we applied the method of Sonnerup and Hasegawa (2005; hereafter SH05) to estimate the invariant axis ($\hat{k}$) of a steady 2D structure and its velocity ($\mathbf{V}_0$) using electric and magnetic field measurements in the GSE coordinates. The SH05 method is based on the principle that the electric field along the invariant axis (i.e., the $\hat{m}$ axis) remains spatially constant within a steady 2D coherent structure. The analysis time interval for the SH05 method is indicated by the two magenta dashed lines in Figure 3, which cover the current sheet crossing. The corresponding results for the three events are summarized in Table 1. Sensitivity tests using slightly different analysis intervals yield consistent SH05 results, with only minor deviations (Table 1). While good agreement is obtained for u_n, a significant discrepancy remains for u_l. We note that for the estimation of the Hall magnetic fields, u_n is the more critical parameter because the contribution associated with j_L is dominant. Therefore, the main conclusions of our analysis are not significantly affected by the uncertainty in u_l.

In Table 1, ϕ_m denotes the angle between $\hat{m}$ and $\hat{k}$. Consistent results are obtained when ϕ_m is small. For G1, however, the angle ϕ_m is moderately large (~36.5°). Using the $\hat{k}$ vector to estimate the Hall magnetic field yields $u_n = -40$ km/s and $u_l = -20$ km/s, consistent with the previous results, and the Hall magnetic field structure remains unchanged (see Figure 6). In this case, $\hat{n} = \hat{l}^* \times \hat{k} = (0.931, 0.196, -0.309)$, $\hat{m} = \hat{k}$, and $\hat{l} = \hat{m} \times \hat{n} = (0.365, -0.456, 0.811)$, which define a new LMN coordinate system, where $\hat{l}^* = (0.360, -0.341, 0.868)$ is the previous L axis. The inferred guide field is ~−2.8 nT, averaged over the analysis interval. Compared with Figure 2b, the upstream guide fields on the two sides of the current sheet differ significantly, contrary to the expectation for a uniform guide field. We note that the $\hat{m}$ axis used in the three event studies is consistent with that obtained from the hybrid minimum variance analysis method employed in MMS reconnection event studies (e.g., S. Eriksson et al., 2016; T. Phan et al., 2018), where $\hat{l}$ denotes the maximum variance direction, $\hat{n}$ is the cross-product normal, and $\hat{m} = \hat{n} \times \hat{l}$.

In Table 1, E_0 denotes the reconnection electric field along the $\hat{k}$ axis. Except for G2, the sign of B_g is consistent with that of E_0. The relative polarity between the guide field and the reconnection electric field may influence the electron dynamics near the electron diffusion region, including electron acceleration or deceleration and the associated field-aligned currents. These effects may, in turn, influence the structure of the Hall magnetic fields. However, a systematic investigation of this dependence requires a dedicated analysis and represents an important topic for future work.

PIC simulations of asymmetric reconnection without a guide field (L. L. Sang et al., 2019a) showed that the hexapolar Hall magnetic field structure evolves from a quadrupolar structure. This transition is driven by additional electron flows moving away from the X-line along magnetic field lines on the magnetosheath side of the current sheet, thereby forming an additional Hall current loop (see Figure 4f). This evolution is enhanced by a large magnetic field ratio (>2.0) and a low plasma density ratio (<0.33) across the current sheet. Although the PIC simulations clearly identify that electron flows as the source of the additional Hall current loop, the fundamental physical mechanism responsible for their formation remains unclear. One may ask whether the asymmetric Hall

Journal of Geophysical Research: Space Physics 10.1029/2026JA035335

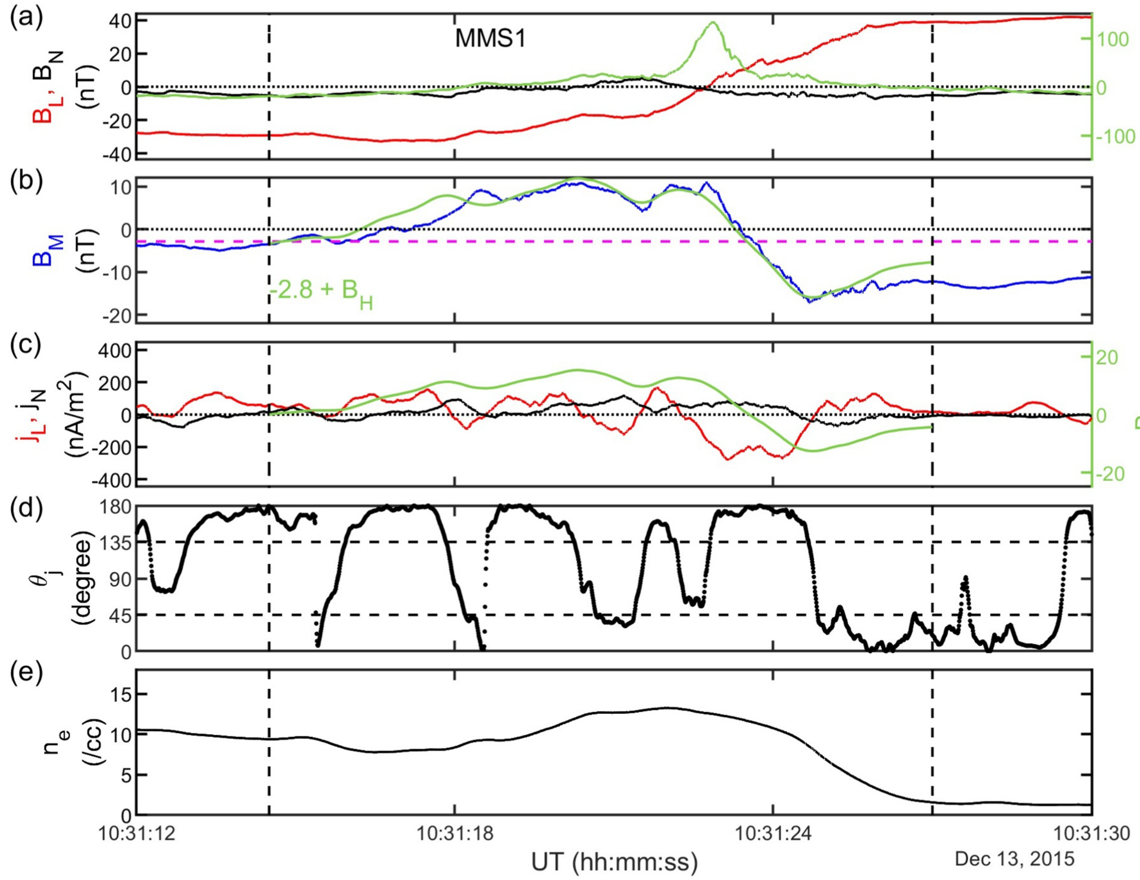

Figure 6. Validation results for the G1 event, in which the Hall magnetic field is estimated using the $\hat{k}$ vector. The panels are presented in the same format as Figure 2.

magnetic field structure represents a transient stage in the evolution from quadrupolar to hexapolar configurations. However, no asymmetric Hall magnetic field structure was observed during this evolution. When a substantial guide field ($\geq 0.2\ B_0$) was introduced into an asymmetric current sheet, this evolution did not occur, and the asymmetric pattern persisted (L. L. Sang et al., 2019b). Specifically, L. L. Sang et al. (2019b) investigated the Hall magnetic field structures for three different guide-field strengths ($B_g/B_0 = 0.2$, 1.0, and 1.5), using fixed upstream magnetic field and density ratios (2.0 and 1/3, respectively). They found that the asymmetric Hall magnetic field pattern persisted in all three cases (see their Figure 3). Overall, these simulation results suggest that the asymmetric pattern may not be a transient phenomenon. A substantial guide field appears to play a key role in producing the asymmetric Hall magnetic-field pattern in an asymmetric reconnecting current sheet.

In conclusion, this study provides the first observational evidence of an asymmetric Hall magnetic field structure in guide-field magnetopause reconnection. Our results support the kinetic predictions of asymmetric electron–ion decoupling and indicate that guide fields play an important role in shaping Hall current systems. These findings provide an observational framework for future investigations of how guide fields influence the conversion of magnetic energy (e.g., Y. K. Shu et al., 2022) and its distribution between electrons and ions during asymmetric reconnection.

Conflict of Interest

The authors declare no conflicts of interest relevant to this study.

Acknowledgments

This work was supported by a grant from Universiti Kebangsaan Malaysia (GP-K020730). Special thanks to all the MMS mission teams for data access.

Availability Statement

MMS data can be downloaded through the NASA CDAWeb at http://cdaweb.gsfc.nasa.gov/. Simulation data are provided by Shu, Y. K., Lu, S. et al. (2022). All analyses were conducted and all plots were generated using MATLAB software, which is available for purchase at https://www.mathworks.com/products/matlab.html.

References

Birn, J., Drake, J. F., Shay, M. A., Rogers, B. N., Denton, R. E., Hesse, M., et al. (2001). Geospace Environmental Modeling (GEM) magnetic reconnection challenge. *Journal of Geophysical Research*, *106*(A3), 3715–3719. https://doi.org/10.1029/1999JA900449

Burch, J. L., Moore, T. E., Torbert, R. B., & Giles, B. L. (2016). Magnetospheric multiscale overview and science objectives. *Space Science Reviews*, *199*(1–4), 5–21. https://doi.org/10.1007/s11214-015-0164-9

Burch, J. L., & Phan, T. D. (2016). Magnetic reconnection at the dayside magnetopause: Advances with MMS. *Geophysical Research Letters*, *43*(16), 8327–8338. https://doi.org/10.1002/2016GL069787

Dai, L. (2018). Structures of hall fields in asymmetric magnetic reconnection. *Journal of Geophysical Research: Space Physics*, *123*(9), 7332–7341. https://doi.org/10.1029/2018JA025251

Eastwood, J. P., Phan, T. D., Øieroset, M., & Shay, M. A. (2010). Average properties of the magnetic reconnection ion diffusion region in the Earth's magnetotail: The 2001-2005 Cluster observations and comparison with simulations. *Journal of Geophysical Research*, *115*(A8), A08215. https://doi.org/10.1029/2009JA014962

Eastwood, J. P., Phan, T. D., Øieroset, M., Shay, M. A., Malakit, K., Swisdak, M., et al. (2013). Influence of asymmetries and guide fields on the magnetic reconnection diffusion region in collisionless space plasmas. *Plasma Physics and Controlled Fusion*, *55*(12), 124001. https://doi.org/10.1088/0741-3335/55/12/124001

Eriksson, S., Lavraud, B., Wilder, F. D., Stawarz, J. E., Giles, B. L., Burch, J. L., et al. (2016). Magnetospheric multiscale observations of magnetic reconnection associated with Kelvin-Helmholtz waves. *Geophysical Research Letters*, *43*(11), 5606–5615. https://doi.org/10.1002/2016GL068783

Fu, X. R., Lu, Q. M., & Wang, S. (2006). The process of electron acceleration during collisionless magnetic reconnection. *Physics of Plasmas*, *13*(1), 012309. https://doi.org/10.1063/1.2164808

Li, X., Dong, C., Ji, H., Zhang, C., Wang, L., Giles, B., et al. (2025). Observation of a knotted electron diffusion Region in Earth's magnetotail reconnection. *Geophysical Research Letters*, *52*(20), e2025GL117612. https://doi.org/10.1029/2025GL117612

Lindqvist, P.-A., Olsson, G., Torbert, R. B., King, B., Granoff, M., Rau, D., et al. (2016). The spin-plane double probe electric field instrument for MMS. *Space Science Reviews*, *199*(1–4), 137–165. https://doi.org/10.1007/s11214-014-0116-9

Lu, Q. M., Huang, C., Xie, J. L., Wang, R. S., Wu, M. Y., Vaivads, A., & Wang, S. (2010). Features of separatrix regions in magnetic reconnection: Comparison of 2-D particle-in-cell simulations and Cluster observations. *Journal of Geophysical Research*, *115*(A11), A11208. https://doi.org/10.1029/2010JA015713

Lu, S., Lu, Q. M., Cao, Y., Huang, C., Xie, J. L., & Wang, S. (2011). The effects of the guide field on the structures of electron density depletions in collisionless magnetic reconnection. *Chinese Science Bulletin*, *56*(1), 48–52. https://doi.org/10.1007/s11434-010-4250-9

Mozer, F. S., Bale, S. D., & Phan, T. D. (2002). Evidence of diffusion regions at a subsolar magnetopause crossing. *Physical Review Letters*, *89*(1), 015002. https://doi.org/10.1103/PhysRevLett.89.015002

Mozer, F. S., Pritchett, P. L., Bonnell, J., Sundkvist, D., & Chang, M. T. (2008). Observations and simulations of asymmetric magnetic field reconnection. *Journal of Geophysical Research*, *113*(A1), A00C03. https://doi.org/10.1029/2008JA013535

Nagai, T., Shinohara, I., Fujimoto, M., Hoshino, M., Saito, Y., Machida, S., & Mukai, T. (2001). Geotail observations of the Hall current system: Evidence of magnetic reconnection in the magnetotail. *Journal of Geophysical Research*, *106*(A11), 25929–25949. https://doi.org/10.1029/2001JA900038

Øieroset, M., Phan, T. D., Fujimoto, M., Lin, R. P., & Lepping, R. P. (2001). In situ detection of collisionless reconnection in the Earth's magnetotail. *Nature*, *412*(6845), 414–417. https://doi.org/10.1038/35086520

Phan, T. D., Eastwood, J. P., Shay, M. A., Drake, J. F., Sonnerup, B. U. Ö., Fujimoto, M., et al. (2018). Electron magnetic reconnection without ion coupling in Earth's turbulent magnetosheath. *Nature*, *557*(7704), 202–206. https://doi.org/10.1038/s41586-018-0091-5

Pollock, C., Moore, T., Jacques, A., Burch, J., Gliese, U., Saito, Y., et al. (2016). Fast plasma investigation for Magnetospheric Multiscale. *Space Science Reviews*, *199*(1–4), 331–406. https://doi.org/10.1007/s11214-016-0245-4

Pritchett, P. L. (2001). Geospace Environment Modeling magnetic reconnection challenge: Simulations with a full particle electromagnetic code. *Journal of Geophysical Research*, *106*(A3), 3783–3798. https://doi.org/10.1029/1999JA001006

Russell, C. T., Anderson, B. J., Baumjohann, W., Bromund, K. R., Dearborn, D., Fischer, D., et al. (2016). The magnetospheric Multiscale magnetometers. *Space Science Reviews*, *199*(1–4), 189–256. https://doi.org/10.1007/s11214-014-0057-3

Sang, L. L., Lu, Q. M., Wang, R. S., Huang, K., & Wang, S. (2018). Quadrupolar and hexapolar Hall magnetic field during asymmetric magnetic reconnection without a guide field. *Physics of Plasmas*, *25*(6), 062120. https://doi.org/10.1063/1.5030439

Sang, L. L., Lu, Q. M., Wang, R. S., Huang, K., & Wang, S. (2019a). A parametric Study of the structure of Hall magnetic field based on kinetic simulations. I. Anti-parallel magnetic Reconnection in an asymmetric Current sheet. *The Astrophysical Journal*, *877*(2), 155. https://doi.org/10.3847/1538-4357/ab14ef

Sang, L. L., Lu, Q. M., Wang, R. S., Huang, K., & Wang, S. (2019b). A parametric Study of the structure of Hall magnetic field based on kinetic simulations. II. Asymmetric magnetic reconnection with a guide field. *The Astrophysical Journal*, *882*(2), 126. https://doi.org/10.3847/1538-4357/ab35d9

Shay, M. A., Drake, J. F., Rogers, B. N., & Denton, R. E. (2001). Alfvénic collisionless magnetic reconnection and the Hall term. *Journal of Geophysical Research*, *106*(A3), 3759–3772. https://doi.org/10.1029/1999JA001007

Shay, M. A., Phan, T. D., Haggerty, C. C., Fujimoto, M., Drake, J. F., Malakit, K., et al. (2016). Kinetic signatures of the region surrounding the X line in asymmetric (magnetopause) reconnection. *Geophysical Research Letters*, *43*(9), 4145–4154. https://doi.org/10.1002/2016GL069034

Shu, Y. K., Lu, S., Lu, Q. M., Wang, R. S., Zheng, J., & Ding, W. X. (2022). Effects of guide field and background density and temperature on energy conversion at magnetic reconnection front. *Journal of Geophysical Research: Space Physics*, *127*(9), e30546. https://doi.org/10.1029/2022JA030546

Sonnerup, B. U. Ö. (1979). Space plasma physics: Magnetic field reconnection (Vol. *3*).46.

Sonnerup, B. U. Ö., & Hasegawa, H. (2005). Orientation and motion of two-dimensional structures in a space plasma. *Journal of Geophysical Research*, *110*(A6), A06208. https://doi.org/10.1029/2004JA010853

Tang, S. Y., Zhang, Y. C., Dai, L., Chen, T., & Wang, C. (2021). MMS observation of the hall field in an asymmetric magnetic reconnection with guide field. *The Astrophysical Journal*, *922*(2), 96. https://doi.org/10.3847/1538-4357/ac31b1

Teh, W.-L., Eriksson, S., Sonnerup, B. U. Ö., Ergun, R., Angelopoulos, V., Glassmeier, K.-H., et al. (2010). THEMIS observations of a secondary magnetic island within the Hall electromagnetic field region at the magnetopause. *Geophysical Research Letters*, *37*(21), L21102. https://doi.org/10.1029/2010GL045056

Teh, W.-L., Nakamura, R., Karimabadi, H., Baumjohann, W., & Zhang, T. L. (2014). Correlation of core field polarity of magnetotail flux ropes with the IMF by: Reconnection guide field dependency. *Journal of Geophysical Research: Space Physics*, *119*(4), 2933–2944. https://doi.org/10.1002/2013JA019454

Teh, W.-L., Nakamura, R., Sonnerup, B. U. Ö., Eastwood, J. P., Volwerk, M., Fazakerley, A. N., & Baumjohann, W. (2011). Evidence of the origin of the Hall magnetic field for reconnection: Hall MHD reconstruction results from Cluster observations. *Journal of Geophysical Research*, *116*(A11), A11218. https://doi.org/10.1029/2011JA016991

Wang, R. S., Nakamura, R., Lu, Q. M., Baumjohann, W., Ergun, R. E., Burch, J. L., et al. (2017). Electron-Scale quadrants of the Hall magnetic field observed by the magnetospheric Multiscale spacecraft during asymmetric reconnection. *Physical Review Letters*, *118*(17), 175101. https://doi.org/10.1103/PhysRevLett.118.175101

Wang, R. S., Nakamura, R., Lu, Q. M., Du, A. M., Zhang, T. L., Baumjohann, W., et al. (2012). Asymmetry in the current sheet and secondary magnetic flux ropes during guide field magnetic reconnection. *Journal of Geophysical Research*, *117*(A7), A07223. https://doi.org/10.1029/2011JA017384

Zhang, Y. C., Lavraud, B., Dai, L., Wang, C., Marchaudon, A., Avanov, L., et al. (2017). Quantitative analysis of a Hall system in the exhaust of asymmetric magnetic reconnection. *Journal of Geophysical Research: Space Physics*, *122*(5), 5277–5289. https://doi.org/10.1002/2016JA023620

Zhou, M., Berchem, J., Walker, R. J., El-Alaoui, M., Goldstein, M. L., Lapenta, G., et al. (2018). Magnetospheric multiscale observations of an ion diffusion Region with large guide field at the magnetopause: Current System, electron heating, and plasma waves. *Journal of Geophysical Research: Space Physics*, *123*(3), 1834–1852. https://doi.org/10.1002/2017JA024517